RSC Advances

PAPER

View Article Online
View Journal | View Issue

Cite this: *RSC Adv.*, 2023, **13**, 30443

Oxygen-doped antimonene monolayer as a promising anchoring material for lithium–sulfur batteries: a first-principles study

Victor Zhu and Xuan Luo *

Received 22nd August 2023
Accepted 10th October 2023

DOI: 10.1039/d3ra05741k

rsc.li/rsc-advances

To effectively mitigate the dissolution of lithium polysulfides (Li_2S_x) in the electrolyte, the search for an effective anchoring material is crucial. In this study, we employed density functional theory (DFT) computations to investigate the adsorption behavior of long-chain Li_2S_x species on an O-doped antimonene monolayer. Our results demonstrate that the O-doped antimonene mono-layer exhibits stronger adsorption for long-chain Li_2S_x species compared to the pristine antimonene monolayer, resulting in enhanced adsorption energies. This improved adsorption effectively curtails the dissolution of lithium polysulfides and preserves the structural integrity of the Li_2S_x species. The charge transfer analysis also revealed the strong chemical interactions between the Li_2S_x species and the O-doped antimonene monolayer. These findings suggest that the O-doped anti-monene monolayer holds promise as an effective anchoring material for enhancing the performance of lithium–sulfur batteries.

I. Introduction

To meet the ever-increasing global energy consumption[1,2] and accommodate the grow-ing use of electric devices, electric vehicles, and renewable energy sources,[3–5] the develop-ment of high-performance rechargeable batteries is desirable. Currently, lithium-ion batter-ies (LIBs) are the optimal rechargeable battery, featuring excellent environmental compat-ibility, high energy density, and long cycle life.[6,7] However, LIBs have limited applications in electric vehicles due to safety, durability, and cost considerations.[4,6,8] In fact, LIBs are approaching their theoretical energy density limit.[9,10] As a potential alternative, lithium–sulfur (Li–S) batteries have gathered great interest due to their higher energy density and theoretical capacity.[11,12] Furthermore, the natural abundance, low cost, and non-toxicity of sulfur make the development of Li–S batteries more attractive.[13,14] Yet the practical ap-plication of lithium–sulfur batteries is impeded by multiple major obsta-cles.[15] One critical issue is the dissolution of soluble long-chain lithium polysulfides (Li_2S_x, $x = 4$, 6, 8) in the electrolyte during the charge/discharge process. The phenomenon referred to as the shuttle effect results in the loss of active materials, rapid capacity fade, and self-discharge.[16–18]

Extensive research has been performed to inhibit the shuttle effect, and various strategies have been proposed to suppress it. One effective strategy is to use anchoring materials to bind lithium polysulfides onto their surface through physical/chemical interactions.[19] Many anchoring materials have been studied, including various carbon materials such as carbon composites,[20] carbon heterostructures[21] because of their high conductivity and large surface area. However, these carbon materials exhibited weak interaction with lithium polysulfides, making them ineffective in fully suppressing the shuttle effect.[22,23] Many other functional materials have also been studied, including polymers,[24,25] metal oxides and sulfides,[26] metal organic frameworks,[27,28] and other metal compounds.[29] Although these functional materi-als have demonstrated strong chemical adsorption strength with lithium polysulfides, their reversible capacity and cycle stability remain unsatisfactory.[30,31] In light of this, previous studies have demonstrated that two-dimensional,[32–34] with their unique electronic properties,[35,36] high surface-volume ratio,[37] and multiple adsorption sites[38] are promising anchoring materials.

Various two-dimensional materials have been investigated to anchor lithium polysul-fides, including transition metal sulfides (*e.g.* TiS_2,[32] VS_2,[33] WS_2 (ref. 34)), other metal com-pounds (*e.g.* SiC_2,[39] V_2CS_2,[40] Ti_2C[41]) and monoelemental two-dimensional materials (*e.g.* borophene,[42] phosphorene,[43] arsenene,[44] and bismuthene[44]). Many of them exhibit weak interactions with lithium polysulfides. Therefore, further studies have explored several ap-proaches to enhance the adsorption strength of lithium polysulfides onto two-dimensional materials. With vacancies, substitution doping of atoms, and surface functionalizations with atom and mole-cules, these methods not only improved the adsorption capa-bility of two-dimensional materials but also exposed more adsorption sites.[34,45,46] For example, N-doping of graphene,[47] transition metal doping of C_2N,[48] and S-termination of Ti_2C Mxene[41] have all improved their adsorption capabilities. As

National Graphene Research and Development Center, Springfield, Virginia 22151, USA. E-mail: xluo@ngrd.org

such, the use of these strategies are of great interest towards strengthening the performance of anchoring materials.

One promising anchoring material for Li–S batteries is antimonene. Due to its moderate band gap,[49] high carrier mobility,[50,51] and high structural stability at ambient temperatures,[46,52] antimonene is promising for application in energy storage. While pre-vious research has demonstrated its effectiveness as an electrode material for LIBs[53] and sodium-ion batteries,[54] recent studies have explored its potential for Li–S batteries.[44,49] However, pristine antimonene exhibits only weak to moderate adsorption capabilities of anchoring lithium polysulfides in Li–S batteries.[44] To overcome this limitation, researchers have turned to doping strategies, with vanadium, tin, and selenium dopants showing promis-ing results through atom substitution.[49] Nevertheless, concerns remain about the strength of adsorption and potential detachment of the adsorbed polysulfides from the doped an-choring material.[55] To address this challenge, oxygen doping has shown promise. Studies involving oxygen doping, such as carbon nitride tubes, revealed improved adsorption of lithium polysulfides through chemical interactions upon substantial oxygen doping.[56–58] Furthermore, doping can decrease the band gap of the monolayer and enhance the intrinsic conductivity, facilitating better lithium diffusion.[59] Thus, we aim to study the adsorption of lithium polysulfides on oxygen-doped antimonene monolayer, potentially improving the performance and stability of Li–S batteries.

We performed first-principle calculations based on Density Functional Theory (DFT) to study the structural and electronic properties of lithium polysulfides adsorbed on pure and doped antimonene. The adsorption energies of the lithium polysulfides adsorbed on pure and oxygen-doped antimonene were calculated to study the suppression of the shuttle effect. In addition to adsorption energies, the band structure, and charge transfer were calculated.

II. Methods

A. Computational details

We performed first-principle calculations based on Density Functional Theory (DFT) within the Perdew–Burke–Ernzerhof (PBE) Generalized Gradient Approximation (GGA) implemented in the ABINIT[60] code. We used the Projected Augmented Wave (PAW) method[61] with projectors generated with the ATOM code.[62] The cut-off radii are 1.0, 1.5, 1.4, 2.4, 1.6, and 1.9 Bohr, and the electrons configurations are 1s1, [He] 2s2 2p2, [He] 2s2 2p4, [Kr] 5s2 5p3 4d10, 1s2 2s1, and [Ne] 3s2 3p4 for H, C, O, Sb, Li, and S, respectively.

Convergence was carried out to determine the appropriate converged values for the kinetic energy cutoff, Monkhorst–Pack k point grids, and vacuum. The values were considered converged when the difference in total energy was less than 1.0×10^{-4} Hartree twice consecutively.[63] During the convergence calculations, the self-consistent field (SCF) total energy calculations were considered complete when the total energy difference was less than 1.0×10^{-10} Hartree for the second time.[63]

The Broyden–Fletcher–Goldfarb–Shanno[64] (BFGS) method was used for the relax-ation of the lattice parameters and atomic structure. During relaxation calculations, SCF iterations were completed when the total difference in forces was less than 2.0×10^{-5} Hartree Bohr^{-1} twice consecutively. The relaxation calculations were considered complete when all of the forces were less than 6.0×10^{-4} Hartree Bohr^{-1} (around 0.03 eV Å^{-1}).[65]

B. Atomic structure

Monolayer antimonene exists in several allotropes, differentiated by their prefixes, α, β, γ, and others.[46] It has been predicted by phonon dispersion spectra, mechanically, and thermally that the α- and β-phases are stable and semiconducting and β-phase is the most stable allotrope.[66]

Previous studies demonstrated β-phase antimonene has nonplanar structure and hexagonal arrangement.[66] In this study, a $4 \times 4 \times 1$ supercell of β-phase antimonene with 32 Sb atoms was used for calculations. We will be substitutionally doping the monolayer with O to enhance its effects on the adsorption of long-chain lithium polysulfides Li_2S_4, Li_2S_6, and Li_2S_8. The defect formation energy (E_{form})[67] is defined by

$$E_{form} = E_{OSbML} - E_{SbML} - E_O + E_{Sb} \quad (1)$$

where E_{OSbML} is the total energy of the O-doped antimonene monolayer, E_{SbML} is the total energy of the pristine antimonene monolayer, E_O is the chemical potential of the O atom, and E_{Sb} is the chemical potential of the Sb atom.

C. Li_2S_x adsorption

To demonstrate the adsorption capabilities of the antimonene monolayer, the ad-sorption energies of Li_2S_x ($x = 1, 2, 4, 6, 8$) with the typical electrolytes dimethyl ether (DME)/1,3-dioxolane (DOL) were calculated with the following equation

$$E_{bind} = E_{LiPS+electro} - E_{LiPS} - E_{electro} \quad (2)$$

where $E_{LiPS+electro}$ is the total energy of the lithium polysulfide and electrolyte DME/DOL complex, E_{LiPS} is the total energy of the Li_2S_x ($x = 1, 2, 4, 6, 8$), and $E_{electro}$ is the total energy of the electrolyte DME/DOL.

Alongside this, the adsorption energies E_{ads} of long-chain lithium polysulfides Li_2S_x ($x = 4, 6, 8$) on the pristine and O-doped antimonene monolayers were calculated by the following equation

$$E_{ads} = E_{LiPS+ML} - E_{ML} - E_{LiPS} \quad (3)$$

where $E_{LiPS+ML}$ is the total energy of the lithium polysulfide and pristine or O-doped antimonene monolayer complex, E_{ML} is the total energy of the pristine or O-doped anti-monene monolayer, and E_{LiPS} is the total energy of the Li_2S_x ($x = 4, 6, 8$), respectively.

D. Electronic structure

The band structure of the antimonene system was calculated before and after the adsorption of Li_2S_x ($x = 4, 6, 8$) polysulfides,

and it was plotted using the high symmetry k-points Γ (0, 0, 0) M (1/2, 0, 0) K (2/3, 1/3, 0) and Γ (1, 1, 1).

The interaction between adsorbed Li_2S_x (x = 4, 6, 8) and O-doped antimonene was further confirmed by calculating the charge transfer. The charge transfer $\Delta\rho(r)$ is defined by

$$\Delta\rho(r) = \rho_{LiPS/OSbML}(r) - \rho_{OSbML}(r) - \rho_{LiPS}(r) \quad (4)$$

where $\rho_{LiPS/OSbML}(r)$ is the charge density of the lithium polysulfide-adsorbed antimonene monolayer system, $\rho_{OSbMl}(r)$ is the charge density of the O-doped antimonene monolayer, and $\rho_{LiPS}(r)$ is the charge density of the lithium polysulfide.

III. Results and discussion

We carried out first-principle calculations to investigate the adsorption of lithium poly-sulfides species on commonly used electrolytes DME and DOL molecules, and both pristine and oxygen-doped antimonene monolayers. We fully relaxed the atomic structures and cal-culated the adsorption energy, band structure, as well as charge transfer.

A. Adsorption of Li_2S_x species on typical electrolytes

1. Atomic structural properties of Li_2S_x species. To mitigate the shuttle effect within Li–S batteries, understanding the formation of lithium polysulfides is critical. During the discharge process, Li is oxidized and travels to-ward the cathode. The reaction between the Li ions and different sulfur concentrations form lithium polysulfides: Li_2S_x (x = 1, 2, 4, 6, 8).[68–70] The molecular models of Li_2S_x (x = 1, 2, 4, 6, 8) were taken from previous research.[71] First, we examined the structural properties of the lithium polysulfides. The most stable configurations after geometric op-timization/relaxation are shown in Fig. 1. The insoluble species Li_2S and Li_2S_2 have a Li–S bond length of 2.22 and 2.34 Å. The soluble Li_2S_4, Li_2S_6, and Li_2S_8 with shortest bond lengths of Li–S and S–S of about 2.38, and 2.08 Å, respectively. In addition, it is found that all of these species are three-dimensional rather than linear, which is consistent with previ-ous theoretical studies.[70] As shown in Table 1, the Li–Li distance decreases, while the Li–S bond distance increases when the number of S atoms increases. Not only this, the Li–S–Li bond angle decreases as the number of S atoms increased, meaning the molecules thickness decreases with the addition of S. Overall, the structural data of lithium polysulfides, as shown in Table 1, are in good agreement with previous theoretical calculations,[72–74] sug-gesting our methods are reliable. Long-chain lithium polysulfides Li_2S_4, Li_2S_6, and Li_2S_8, were selected due to their high solubility in the organic electrolytes leading to large capacity fading during the cycling or the shuttle effect.[75,76] In comparison, the short-chain lithium polysulfides Li_2S and Li_2S_2 are insoluble in the typical electrolytes DOL and DME, which is why we did not complete further research.[75,76]

2. Atomic structural properties of typical electrolytes DME and DOL. The electrolyte is also critical to the electrochemical performance of Li–S batteries, as it governs the movement of lithium ions between the electrodes during charging and discharg-ing. Additionally, the electrolyte plays a crucial role in forming a stable solid electrolyte interphase (SEI) with the electrodes, which significantly impacts battery performance.[77,78] Extensive experimentation has led to the standard electrolyte formulation: a 1 : 1 mixture of dimethyl ether (DME) and 1,3-dioxolane (DOL). This combination exhibits superior reactivity with polysulfides, ensuring enhanced stability and improved electrochemical performance in Li–S batteries.[68,79,80]

The optimized structure of DME and DOL are shown in Fig. 1. DME consists of a central ethane backbone with a methyl ($-CH_3$) group attached to each of the carbon atoms. The calculated C–O–C bond angle after relaxation was measured to be 112.13°, indicating a bent molecular geometry, which is in good agreement with the experimentally calculated angle of approximately 111.43°.[81] DOL adopts a puckered five-member ring, where the ring is not perfectly planar but instead exhibits slight deviation from planarity. The bond lengths between the carbon and oxygen atoms in DOL are relatively equal about 2.7 Å.

3. Adsorption of Li_2S_x species on typical electrolytes. To investigate the adsorption of lithium polysulfides on commonly used electrolytes (DME/DOL), we calculated the structural properties of lithium polysulfides and DME/DOL, which is shown in Fig. 2. For DOL, the shortest intermolecular distance between Li and O is 2.04, 2.02, 2.15, 1.92, and 1.94 Å for Li_2S, Li_2S_2, Li_2S_4, Li_2S_6, and Li_2S_8, respectively. The shortest intermolecular distance between Li_2S, Li_2S_2, Li_2S_4, Li_2S_6, and Li_2S_8 and DME is 1.99 Å, 1.92 Å, 2.01 Å, 2.01 Å, and 2.01 Å respectively. To compare, the Li atoms are closer to the O atoms than the S atoms when interacting with both DOL and DME. In addition, the shortest distances are approximately the sum of the covalaent radii between Li atom and O atom. Therefore, the Li_2S_x species and typical electrolytes tend to form Li–O bonds, which demonstrates that the interaction between the lithium polysulfide species and electrolytes is partially due to chemical interaction.

The adsorption energies of lithium polysulfides on DME and DOL are summarized in Table 2. The adsorption energies of Li_2S, Li_2S_2, Li_2S_4, Li_2S_6, and Li_2S_8 on DOL are −0.83, −0.94, −0.78, −0.69, and −1.05 eV respectively. For DME, the adsoprtion energies of Li_2S, Li_2S_2, Li_2S_4, Li_2S_6, and Li_2S_8 are −0.94, −0.73, −0.62, −1.05, and −0.77 eV, respectively. The adsorption energies between the lithium polysulfides and electrolytes range of −0.69 to −1.05 eV for DOL, and −0.62 to −1.05 eV for DME, showing that the adsorption of lithium polysulfides on DME and DOL do not significantly differ. Therefore, the preferable range of adsorption energies would be from around −1.00 eV to −2.00 eV, as extreme adsorption can hinder the detachment of adsorbed lithium polysulfide from the anchoring material.[82]

B. Adsorption of Li_2S_x species on pristine antimonene monolayer

1. Atomic structural and electronic properties of pristine antimonene monolayer. Fig. 3 shows the 4 × 4 × 1 antimonene monolayer, where two Sb atoms make up a unit cell, which are stacked in a zigzag monolayer. Each Sb atom binds with three

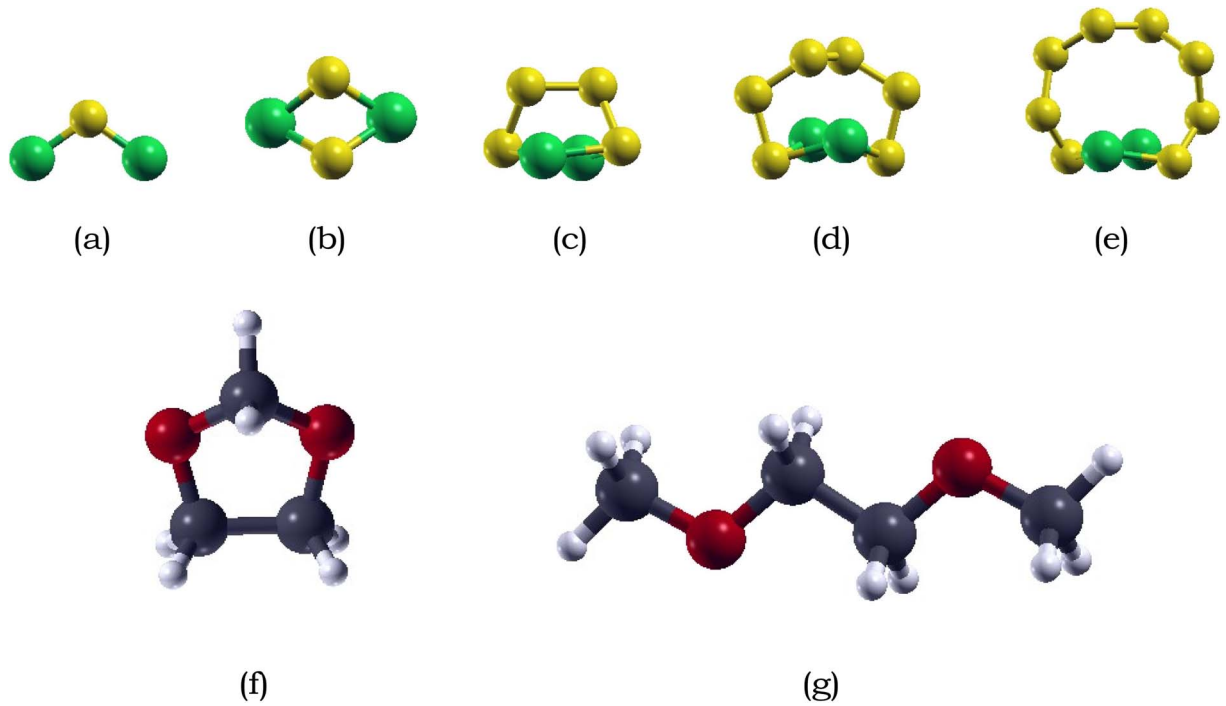

Fig. 1 Optimized atomic structures of Li_2S_x ($x = 1, 2, 4, 6, 8$) and electrolytes DME/DOL: (a) Li_2S, (b) Li_2S_2, (c) Li_2S_4, (d) Li_2S_6, (e) Li_2S_8 (f) DOL, and (g) DME. H, O, C, Li and S atoms are represented by white, red, blue, green, and yellow, respectively.

Table 1 The optimized structural parameters of Li_2S_x ($x = 1, 2, 4, 6, 8$): bond length of S–S (d_{S-S}), bond length of Li–S (d_{Li-S}), bond angle of Li–S–Li ($\theta_{Li-S-Li}$), and bond distance of Li–Li (d_{Li-Li}) in Li_2S_x ($x = 1, 2, 4, 6, 8$)

Species	Li_2S	Li_2S_2	Li_2S_4	Li_2S_6	Li_2S_8
d_{S-S} (Å)	—	2.19	2.09	2.04	2.08
d_{S-S} (Å)	—	2.19[a]	2.19[a]	2.08[a]	2.07[a]
d_{S-S} (Å)	—	—	2.141[b]	2.261[b]	2.087[b]
d_{Li-S} (Å)	2.09	2.22	2.34	2.38	2.38
d_{Li-S} (Å)	2.09[a]	2.22[a]	2.48[a]	2.55[a]	2.42[a]
d_{Li-S} (Å)	2.073[b]	2.227[b]	2.377[b]	2.407[b]	2.412[b]
d_{Li-S} (Å)	2.09[c]	2.23[c]	2.36/2.40[c]	2.35/2.41[c]	2.38/2.39[c]
$\theta_{Li-S-Li}$ (deg)	109.3	95.32	77.38	68.65	66.25
$\theta_{Li-S-Li}$ (deg)	131.8[c]	96.8[c]	73.5[c]	69.1[c]	66.3[c]
d_{Li-Li} (Å)	3.41	3.28	2.82	2.67	2.59

[a] Ref. 71. [b] Ref. 72. [c] Ref. 73.

adjacent atoms in a different plane. Due to the same bond angle of 91.42° between Sb atoms, the monolayer has hexagonal arrangement. The fully relaxed lattice parameters of the pristine antimonene monolayer is $a = b = 4.12$ Å and the bond length between Sb–Sb is found to be 2.89 Å, as presented in Table 5. Overall, our calculated values of the lattice parameters and bond lengths are in good agreement with previously reported works.[49]

Due to the insulating nature of sulfur, an ideal anchoring material for the Li–S battery should possess excellent electronic conductivity, which will greatly affect the performance and operability of the battery. Therefore, we have computed the electronic band structure to understand the electronic properties of antimonene. The monolayer exhibits a band gap of 1.52 eV, as presented in Table 5. The monolayer is an indirect band gap semiconductor between the Γ and M points, as presented in Fig. 3.

2. Adsorption of Li_2S_x species on pristine antimonene monolayer. An optimal anchoring material for Li–S batteries should be able to immobilize lithium polysulfides effectively with strong chemical adsorption. However, extreme adsorption is also undesirable as large adsorption energies, greater than 3.00 eV, can impede the charge/discharge process and cause deformation of polysulfides.[71] Following previous research, we adsorbed the long-chain polysulfides Li_2S_x ($x = 4, 6, 8$) onto pristine antimonene monolayer.[49] The optimized configurations of Li_2S_x ($x = 4, 6, 8$) on the antimonene mono-layer are shown in Fig. 4a–c, respectively.

For Li_2S_4 adsorption, the Li atoms face downwards towards the monolayer, while for Li_2S_6 and Li_2S_8 adsorption, the S chain is parallel to the monolayer surface. The shortest intermolecular distance between Li_2S_6, Li_2S_6, and Li_2S_8 and the antimonene monolayer is 2.93, 2.98, and 3.16 Å, respectively. Specifically, the Li atoms are closer than the S atoms when interacting with the antimonene monolayer, and the two Li atoms prefer to adsorb around the hexagonal edges of antimonene through Li–Sb interactions.

We also calculated the variances of the corresponding structural parameters for both Li_2S_x and pristine antimonene as summarized in Table 3. The average change of the Li–S bond in Li_2S_4, Li_2S_6, and Li_2S_8 is 0.04, 0.02, and 0.07 Å. Not only this, for the antimonene monolayer, the nearby Sb–Sb bonds increased

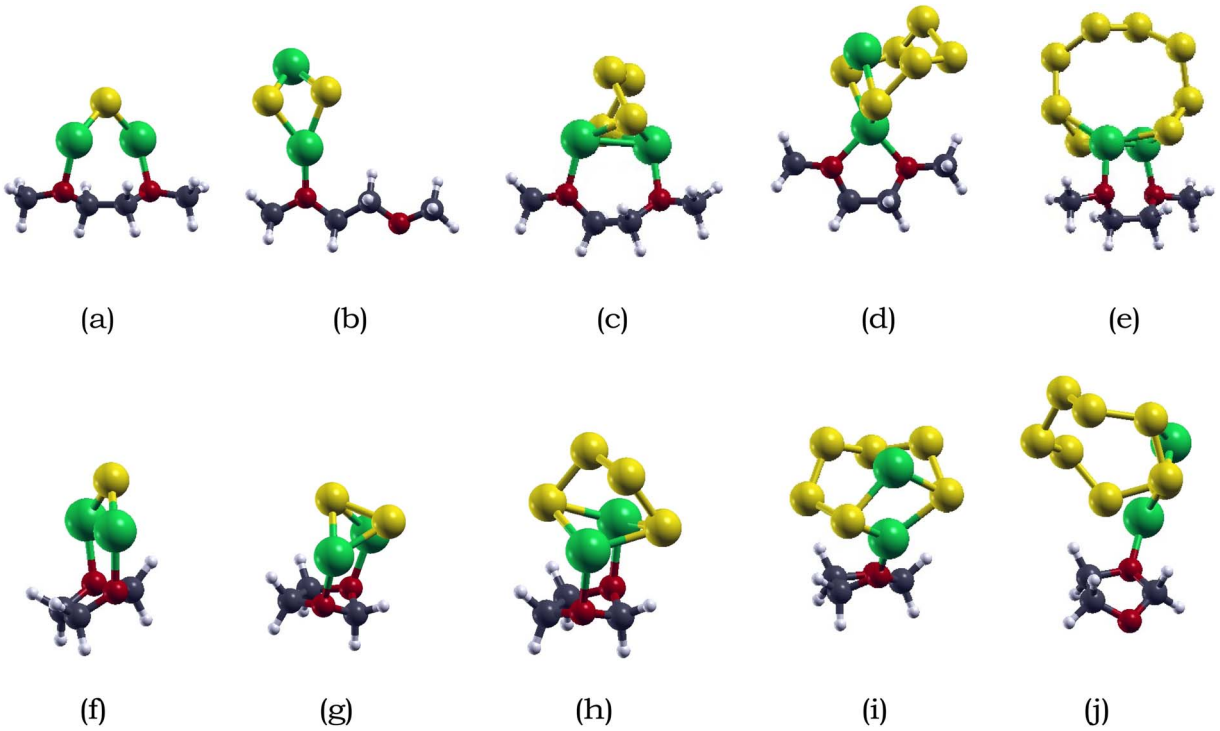

Fig. 2 Optimized atomic structures of Li_2S_x ($x = 1, 2, 4, 6, 8$) adsorbed with electrolytes DME/DOL: (a) Li_2S + DME, (b) Li_2S_2 + DME, (c) Li_2S_4 + DME, (d) Li_2S_6 + DME, (e) Li_2S_8 + DME, (f) Li_2S + DOL, (g) Li_2S_2 + DOL, (h) Li_2S_4 + DOL, (i) Li_2S_6 + DOL, (j) Li_2S_8 + DOL. H, O, C, Li, and S atoms are represented by white, red, blue, green and yellow.

Table 2 The binding energy E_{bind} (eV) of Li_2S_x ($x = 1, 2, 4, 6, 8$) molecules with DME and DOL molecules

	Li_2S	Li_2S_2	Li_2S_4	Li_2S_6	Li_2S_8
E_{bind}-DME (eV)	−0.94	−0.73	−0.62	−1.05	−0.77
E_{bind}-DOL (eV)	−0.83	−0.94	−0.78	−0.69	−1.05

only around 0.01 Å. Therefore, little structural deformation is observed for both the adsorbed long-chain lithium polysulfides and the antimonene monolayer, which is preferable as severe deformation away from the stable configuration is unfavorable.[83]

The adsorption energies of the Li_2S_x ($x = 4, 6, 8$) species on antimonene are listed in Table 4. The adsorption energies of Li_2S_4, Li_2S_6, and Li_2S_8 on the antiomonene monolayer are

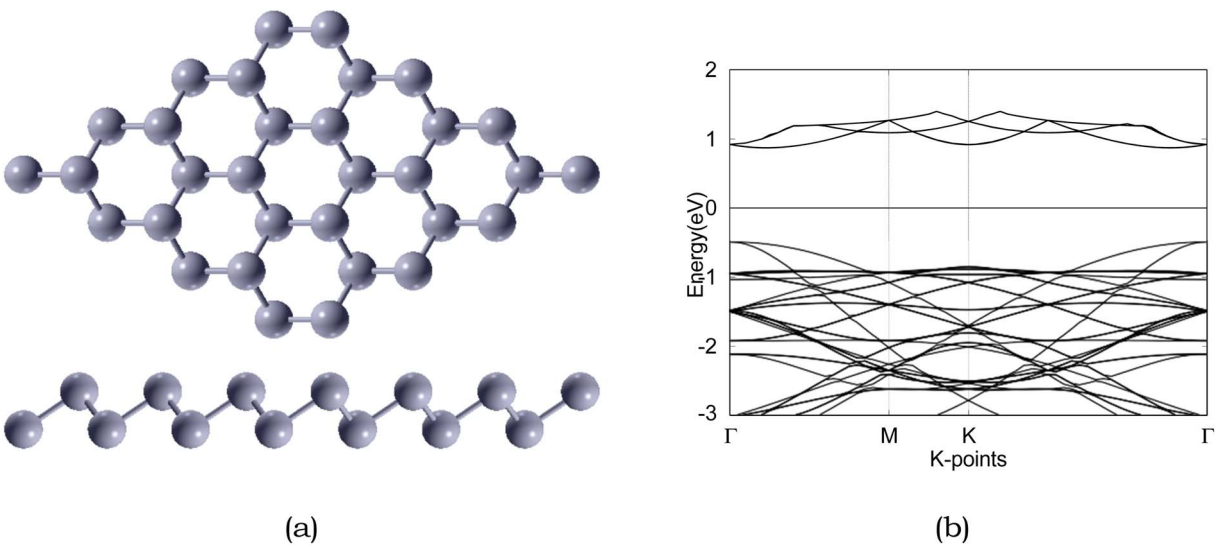

Fig. 3 Atomic structure and band structure of 4 × 4 × 1 pristine. The Fermi level is set to 0. Sb is represented by silver, respectively.

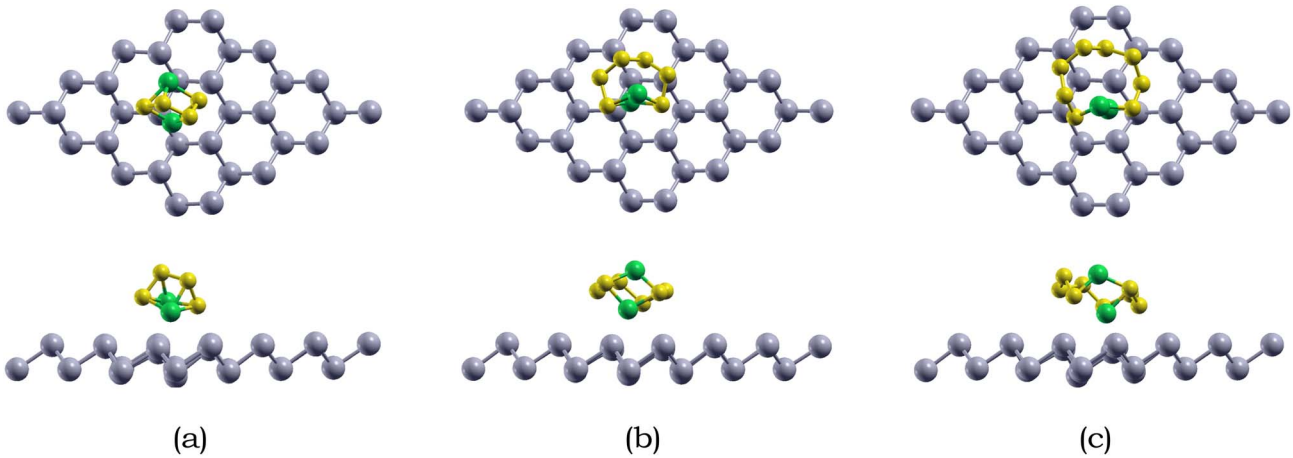

Fig. 4 Top and side views of the optimized atomic structures Li_2S_x ($x = 4, 6, 8$) adsorbed on 4 × 4 × 1 pristine antimonene monolayer: (a) Li_2S_4, (b) Li_2S_6, and (c) Li_2S_8. Sb, Li, and S are represented by silver, green, and yellow, respectively.

Table 3 The shortest distance between Li_2S_x ($x = 4, 6, 8$) and pristine antimonene monolayer d_{Sb-Li}, the change of the distance between Li and S atoms in Li_2S_x ($x = 4, 6, 8$) Δd_{Li-S}, and the change in the bond length between Sb and Sb atoms in pristine antimonene monolayer Δd_{Sb-Sb}

Species	d_{Sb-Li} (Å)	Δd_{Li-S} (Å)	Δd_{Sb-Sb} (Å)
Li_2S_4	2.93	0.04	0.01
Li_2S_6	2.98	0.02	0.01
Li_2S_8	3.16	0.07	0.01

Table 4 Adsorption energy E_{ads} (eV) of Li_2S_x ($x = 4, 6, 8$) on both pristine antimonene (SbML) and O-doped antimonene monolayer (OSbML) substrates

LiPS	Li_2S_4	Li_2S_6	Li_2S_8
E_{ads}-SbML (eV)	−0.90	−0.82	−0.70
E_{ads}-SbML (eV)	−1.01[a]	−1.164[a]	−1.40[a]
E_{ads}-OSbML (eV)	−1.24	−1.21	−1.12

[a] Ref. 49.

−0.90, −0.82, and −0.70 eV, respectively. The overall adsorption energies of antimonene to the Li_2S_x ($x = 4, 6, 8$) species range from −0.70 to −0.90 eV, which are similar to previous results.[49]

C. Adsorption of Li_2S_x species on O-doped antimonene monolayer

1. Atomic structural and electronic properties of O-doped antimonene monolayer. To further improve the performance of antimonene for applications in Li–S bat-tery, a doping modification was applied. Among the various dopants used in previous studies,[41,47–49] oxygen doping has been far less studied and applied for Li–S batteries. However, it has demonstrated success with strong chemical interactions with Li–O bonds forming in its applications in carbon–nitride tubes,[57] carbon nanofiber interlayers,[58] and other carbon materials.[56] Therefore, we doped antimonene with oxygen and evaluated its performance. After geometric optimization, we obtained a stable oxygen-doped antimonene monolayer. As shown in Fig. 5, the oxygen atom coordinates with the 3 adjacent Sb atoms in the corresponding configuration. It can be observed that the O atom slightly deformed the six-member ring near the doping site and shrank into the antimonene monolayer. The O atom shrank into the monolayer due to the smaller atomic radii of O atom than Sb atoms. The calculated O–Sb bond length after relaxation was 2.23. The bond angle of the Sb–O–Sb was found to be 111.09°. The lattice constants was measured to be 4.07 Å decreased from pristine antimonene's lattice constant of 4.12 Å, as presented in Table 5. To evaluate the thermodynamic stability of the oxygen-doped system, the formation energy was calculated using eqn (1). The defect formation energy was calculated to be 1.09 eV, as presented in Table 5. The low positive formation energy demonstrates the applicability of oxygen doping within antimonene, as the small magnitude of the formation energy demonstrates the material should be mechanically stable in a natural environment. Therefore, we further investigated the structural and electronic properties of the doped system. As shown in Fig. 5, the doped monolayer exhibits a band gap of 1.37 eV. The monolayer is an indirect band gap semiconductor between the Γ and M points, as presented in Fig. 5. The re-duced bandgap will increase the electrical conductivity and improve the performance of Li–S batteries.

2. Adsorption of Li_2S_x species on O-doped antimonene monolayer. We first examine the adsorption strength between the Li_2S_x species and the O-doped antimonene monolayer. Various initial adsorption configurations for Li_2S_x ($x = 4, 6, 8$) were considered. The optimized configurations of Li_2S_x ($x = 4, 6, 8$) are shown in Fig. 6a–c, respectively. For Li_2S_4 adsorption, the Li atoms slant downwards towards the monolayer, while for Li_2S_6 and Li_2S_8 adsorption, the S chain is parallel to the monolayer surface. The shortest intermolecular distance between Li_2S_4, Li_2S_6, and Li_2S_8 is 1.95, 1.87, and 1.88 Å, respectively. Specifically, the Li atoms are closer than the S

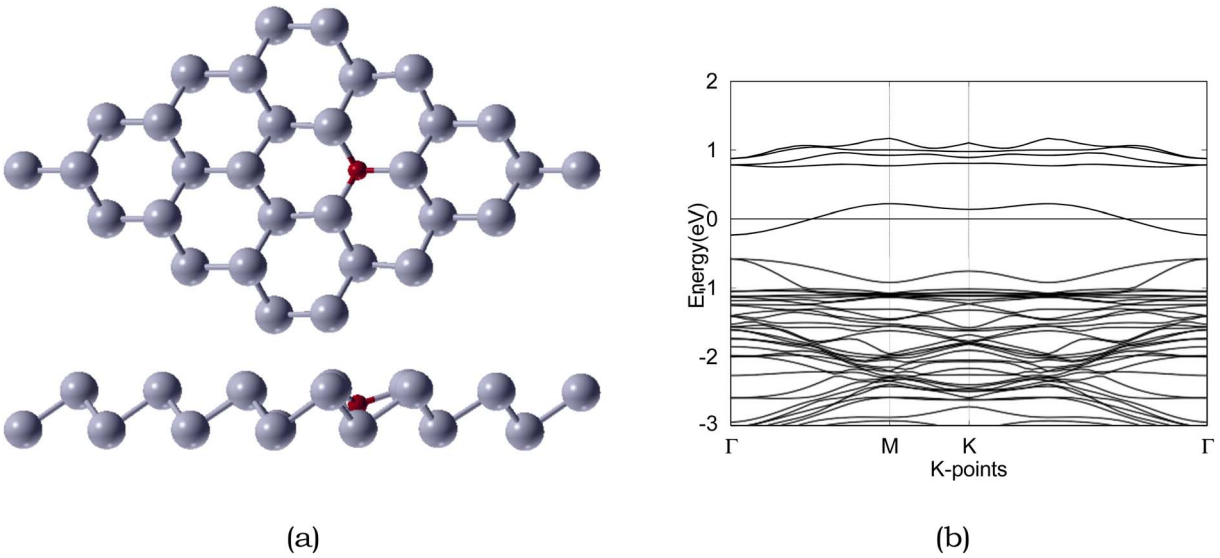

Fig. 5 Atomic structure and band structure of 4 × 4 × 1 O-doped antimonene monolayer. The Fermi level is set to 0. Sb and O are represented by silver and red, respectively.

atoms when interacting with the doped monolayer, and the Li atoms prefer to adsorb around the O atom through Li–O interactions. In addition, for all the long-chain lithium polysulfides the shortest distances are approximately the sum of the covalent radii between the Li atom and Sb atom. Therefore, the Li_2S_x species and the monolayers tend to form Li–O bonds, which confirms the anchoring effect in these adsorption systems has a partial contribution from the chemical interaction. Comparatively, the distances for O-doped antimonene are considerably smaller than that of the pristine antimonene reflecting the stronger interactions between the adsorbate and substrate.

We also calculated the variances of the corresponding structural parameters for both Li_2S_x (x = 4, 6, 8) and the O-doped antimonene monolayer, as summarized in Table 6. The average change of the Li–S bond in Li_2S_4, Li_2S_6, and Li_2S_8 is 0.44, 0.04, and 0.07 Å. Not only this, for the antimonene monolayer, the nearby O–Sb bonds increased around 0.57, 0.43, and 0.47 Å for the adsorption of Li_2S_4, Li_2S_6, and Li_2S_8. The considerable change in the substrate is observed due to the attraction between the Li and O atoms, resulting in the O atom moving away from one of the adjacent Sb atoms to bond with the Li atoms. The variances of the structural parameters of both adsorbates and substrates are considerably larger, indicating that the Li_2S_x species experienced some deformation, but are nearly intact.

The adsorption energies of the Li_2S_x (x = 4, 6, 8) species on O-doped antimonene are listed in Table 4. The adsorption energies of Li_2S_4, Li_2S_6, and Li_2S_8 on the doped monolayer is −1.24, −1.21, and −1.12 eV, respectively. The overall adsorption energies Li_2S_x (x = 4, 6, 8) species adsorbed on O-doped antimonene range from −1.12 to −1.24 eV, stronger than those of pristine antimonene. The higher chemical reactivity between the Li_2S_x species and O-doped antimonene than pristine antimonene is due to the electronegativity difference between Li and O.

Moreover, we compared the energy gain for Li_2S_x species to form large Li–S interconnected clusters (or networks) and the adsorption energies of the Li_2S_x (x = 4, 6, 8) on O-doped antimonene. The energy gain to create interconnected Li_2S_x clusters is less than around 0.40 eV for Li_2S_x (x = 4, 6, 8),[69] which is smaller than the Li_2S_x and O-doped anti-monene interactions (−1.24, −1.21, −1.12 eV, respectively). Consequently, the three long-chain lithium polysulfides generally prefer anchoring on

Table 5 Optimized atomic structure of 4 × 4 × 1 pristine antimonene monolayer (SbML) and O-doped antimonene monolayer (OSbML): lattice constant a (Å), bond length of Sb–Sb in pristine antimonene d_{Sb-Sb} (Å), bond length of O–Sb in O-doped antimonene d_{O-Sb} (Å), bond angle of Sb–Sb–Sb in pristine antimonene $\theta_{Sb-Sb-Sb}$ (deg), bond angle of Sb–O–Sb in O-doped antimonene $\theta_{Sb-Sb-Sb}$ (deg), defect formation energy E_{form} (eV), and bandgap E_g (eV)

Configuration	a (Å)	d_{Sb-Sb} (Å)	d_{O-Sb} (Å)	$\theta_{Sb-Sb-Sb}$ (deg)	$\theta_{Sb-O-Sb}$ (deg)	E_{form} (eV)	E_g (eV)
SbML	4.12	2.89	—	91.42	—	0.00	1.52
SbML	4.07[a]	2.84[a]	—	91.47[a]	—	0.00[a]	1.37[a]
OSbML	4.07	—	2.23	—	111.09	1.07	0.00

[a] Ref. 49.

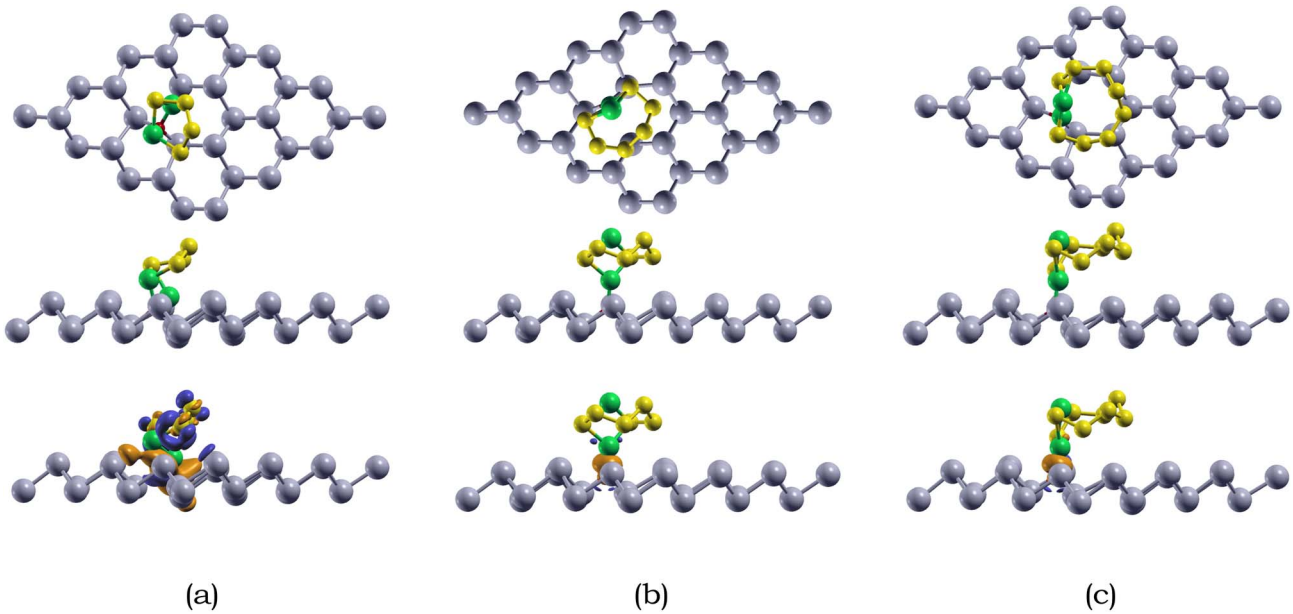

Fig. 6 Top view (1st row) and side view (2nd row) of the optimized atomic structure and charge transfer (3rd row) of Li_2S_x ($x = 4, 6, 8$) species on the O-doped antimonene monolayer (OSbML) (a) Li_2S_4/OSbML (b) Li_2S_6/OSbML, and (c) Li_2S_8/OSbML. The orange and dark blue bubbles represent charge accumulation and depletion, respectively. The isosurface is 0.002 e per Å^3. Sb, O, Li, and S are represented by silver, red, green, and yellow, respectively.

Table 6 The shortest distance between Li_2S_x ($x = 4, 6, 8$) and O-doped antimonene monolayer d_{O-Li}, the change of the distance between Li and S atoms in Li_2S_x ($x = 4, 6, 8$) Δd_{Li-S}, and the change in the bond length between Sb and O atoms in O-doped antimonene monolayer Δd_{Sb-O}

Species	d_{O-Li} (Å)	Δd_{Li-S} (Å)	Δd_{Sb-O} (Å)
Li_2S_4	1.95	0.44	0.57
Li_2S_6	1.87	0.04	0.43
Li_2S_8	1.88	0.07	0.47

O-doped antiomonene than nucleation into larger Li_2S_x clusters. In addition, we compared the binding energy for Li_2S_x species with DME and DOL and the adsorption energies of Li_2S_x ($x = 4, 6, 8$) on O-doped antimonene. The binding energies of the Li_2S_x species with the electrolytes are smaller than those with the O-doped antimonene monolayer. Therefore, it can be seen that the Li_2S_x species would prefer to anchor on the O-doped antimonene monolayer and not dissolve in the electrolyte.

Overall, the adsorption energies of the soluble Li_2S_x species are moderate (−1.00 to −2.00 eV), the adsorbed Li_2S_x species and the O-doped antimonene are nearly intact. Therefore, we expect that O-doped antimonene is suitable as an anchoring material for Li–S batteries.

3. Charge transfer. We also performed charge transfer calculations to investigate the adsorption properties of Li_2S_x ($x = 4, 6, 8$) species on the O-doped antimonene monolayer, following eqn (4). Notably, significant regions of electron accumulation are located between the Li atom of the Li_2S_x species and the O dopant, as depicted in the 2nd row of Fig. 6. There was also minimal charge redistribution in Li_2S_6 and Li_2S_8 compared to Li_2S_4. The enhanced adsorption energy can be explained by the large electronegativity difference between lithium and oxygen. Because of the significant difference in electronegativity between lithium (3.44) and oxygen (0.98), the interaction is very analogous to the "Li bond" explained in the Lewis acid–base theory.[84,85] The O-doped antimonene with an extra pair of electrons is expected as an electron-rich donor that naturally acts as Lewis base sites to strongly absorb Lewis acidic Li ions through acid–base interactions. The significant electron density visible around the lone pairs of the O atoms strengthens the fact that these extra electrons act as electron-rich donors that interact with the strong Li-ion Lewis acid to form a coordinate covalent bond,[86] as shown in the 2nd and 3rd rows of Fig. 6. Overall, our findings confirm the strong chemical interactions between the Li_2S_x species and the O-doped antimonene monolayer, further supporting its potential as an effective anchoring material for Li–S batteries.

IV. Conclusion

By using first-principles calculations based on DFT, the adsorption behavior of Li_2S_x ($x = 4, 6, 8$) species on the pristine and O-doped antimonene monolayers was investigated. The Li_2S_x species were weakly adsorbed on the pristine antimonene monolayer while mod-erately adsorbed on the O-doped antimonene monolayer. Therefore, the Li_2S_x species are adsorbed on the O-doped antimonene monolayer and the dissolution of the Li_2S_x species into the electrolyte is prevented from an energetic point of view. Furthermore, the charge transfer from the Li_2S_x species to the O-doped antimonene monolayer

revealed strong chem–ical interactions between the Li_2S_x species and O-doped antimonene monolayer. Therefore, the O-doped antimonene monolayer is a promising anchoring material for high-performance Li–S batteries.

Conflicts of interest

There are no conflicts to declare.

Acknowledgements

We would like to thank Dr Geifei Qian for his technical support throughout our research.

References

1 L. Pérez-Lombard, J. Ortiz and C. Pout, *Energy Buildings*, 2008, **40**, 394.
2 K. Karpov, *Studies on Russian Economic Development*, 2019, **30**, 38.
3 A. Bloom, U. Helman, H. Holttinen, K. Summers, J. Bakke, G. Brinkman and A. Lopez, *IEEE Power Energy Mag.*, 2017, **15**, 22.
4 M. M. Thackeray, C. Wolverton and E. D. Isaacs, *Energy Environ. Sci.*, 2012, **5**, 7854.
5 Y. Wang, B. Liu, Q. Li, S. Cartmell, S. Ferrara, Z. D. Deng and J. Xiao, *J. Power Sources*, 2015, **286**, 330.
6 B. Scrosati and J. Garche, *J. Power Sources*, 2010, **195**, 2419.
7 M.-Y. Yan, G. Li, J. Zhang, Y.-F. Tian, Y.-X. Yin, C.-J. Zhang, K.-C. Jiang, Q. Xu, H.-L. Li and Y.-G. Guo, *ACS Appl. Mater. Interfaces*, 2020, **12**, 27202.
8 L. Lu, X. Han, J. Li, J. Hua and M. Ouyang, *J. Power Sources*, 2013, **226**, 272.
9 T. C. Wanger, *Conserv. Lett.*, 2011, **4**, 202.
10 K. Abraham, *J. Phys. Chem. Lett.*, 2015, **6**, 830.
11 K. Divya and J. Østergaard, *Electr. Power Syst. Res.*, 2009, **79**, 511.
12 J. Cho, S. Jeong and Y. Kim, *Prog. Energy Combust. Sci.*, 2015, **48**, 84.
13 A. Manthiram, Y. Fu and Y.-S. Su, *Acc. Chem. Res.*, 2013, **46**, 1125.
14 Y. Yang, G. Zheng and Y. Cui, *Chem. Soc. Rev.*, 2013, **42**, 3018.
15 J. Sun, T. Wang, Y. Gao, Z. Pan, R. Hu and J. Wang, *InfoMat*, 2022, **4**, e12359.
16 D. Liu, C. Zhang, G. Zhou, W. Lv, G. Ling, L. Zhi and Q.-H. Yang, *Adv. Sci.*, 2018, **5**, 1700270.
17 J. Yan, X. Liu and B. Li, *Advanced Science*, 2016, **3**, 1600101.
18 Y. V. Mikhaylik and J. R. Akridge, *J. Electrochem. Soc.*, 2004, **151**, A1969.
19 W. Ren, W. Ma, S. Zhang and B. Tang, *Energy Storage Mater.*, 2019, **23**, 707.
20 G. Li, J. Sun, W. Hou, S. Jiang, Y. Huang and J. Geng, *Nat. Commun.*, 2016, **7**, 1.
21 C. Zhang, Q. He, W. Chu and Y. Zhao, *Appl. Surf. Sci.*, 2020, **534**, 147575.
22 L. Chen, H. Zhou, C. Fu, Z. Chen, C. Xu and Y. Kuang, *Int. J. Hydrogen Energy*, 2016, **41**, 21850.
23 Q. Pang, J. Tang, H. Huang, X. Liang, C. Hart, K. C. Tam and L. F. Nazar, *Adv. Mater.*, 2015, **27**, 6021.
24 Y. Fu, Y.-S. Su and A. Manthiram, *J. Electrochem. Soc.*, 2012, **159**, A1420.
25 X. Zhao, C. Wang, Z. Li, X. Hu, A. A. Razzaq and Z. Deng, *J. Mater. Chem. A*, 2021, **9**, 19282.
26 X. Liu, J.-Q. Huang, Q. Zhang and L. Mai, *Adv. Mater.*, 2017, **29**, 1601759.
27 J. Zheng, J. Tian, D. Wu, M. Gu, W. Xu, C. Wang, F. Gao, M. H. Engelhard, J.-G. Zhang, J. Liu, *et al.*, *Nano Lett.*, 2014, **14**, 2345.
28 Y. Hou, H. Mao and L. Xu, *Nano Res.*, 2017, **10**, 344.
29 J. Xu, T. Lawson, H. Fan, D. Su and G. Wang, *Adv. Energy Mater.*, 2018, **8**, 1702607.
30 C. Li, Z. Xi, D. Guo, X. Chen and L. Yin, *Small*, 2018, **14**, 1701986.
31 Y. Zhu, S. Wang, Z. Miao, Y. Liu and S.-L. Chou, *Small*, 2018, **14**, 1801987.
32 W. Zhao, L.-C. Xu, R. Li, Y. Guo, Z. Yang, R. Liu and X. Li, *Mater. Today Commun.*, 2022, **30**, 103196.
33 Y. Wang, Z. Ma, N. Song, T. Zhang, Q. Zhang, D. Yang and F. Wang, *Chem. Phys. Lett.*, 2020, **741**, 137121.
34 R. Jayan and M. M. Islam, *J. Phys. Chem. C*, 2020, **124**, 27323.
35 S. Z. Butler, S. M. Hollen, L. Cao, Y. Cui, J. A. Gupta, H. R. Gutíerrez, T. F. Heinz, S. S. Hong, J. Huang, A. F. Ismach, *et al.*, *ACS Nano*, 2013, **7**, 2898.
36 Q. H. Wang, K. Kalantar-Zadeh, A. Kis, J. N. Coleman and M. S. Strano, *Nat. Nanotechnol.*, 2012, **7**, 699.
37 D. Chimene, D. L. Alge and A. K. Gaharwar, *Adv. Mater.*, 2015, **27**, 7261.
38 H. Xu, Z. Kong, J. Siegenthaler, B. Zheng, Y. Tong, J. Li, T. Schuelke, Q. H. Fan, K. Wang, H. Xu, *et al.*, *EcoMat*, 2023, **5**, e12286.
39 Y. Zhao, J. Zhao and Q. Cai, *Appl. Surf. Sci.*, 2018, **440**, 889.
40 Y. Wang, J. Shen, L.-C. Xu, Z. Yang, R. Li, R. Liu and X. Li, *Phys. Chem. Chem. Phys.*, 2019, **21**, 18559.
41 X. Liu, X. Shao, F. Li and M. Zhao, *Appl. Surf. Sci.*, 2018, **455**, 522.
42 L. Zhang, P. Liang, H.-b. Shu, X.-l. Man, F. Li, J. Huang, Q.-m. Dong and D.-l. Chao, *J. Phys. Chem. C*, 2017, **121**, 15549.
43 H. H. Haseeb, Y. Li, S. Ayub, Q. Fang, L. Yu, K. Xu and F. Ma, *J. Phys. Chem. C*, 2020, **124**, 2739.
44 X. Mao, L. Zhu and A. Fu, *Int. J. Quantum Chem.*, 2021, **121**, e26661.
45 N. Yamsang, J. Sittiwong, P. Srifa, B. Boekfa, M. Sawangphruk, T. Maihom and J. Limtrakul, *Appl. Surf. Sci.*, 2021, **565**, 150378.
46 G. Wang, R. Pandey and S. P. Karna, *ACS Appl. Mater. Interfaces*, 2015, **7**, 11490.
47 G. S. Yi, E. S. Sim and Y.-C. Chung, *Phys. Chem. Chem. Phys.*, 2017, **19**, 28189.
48 H. Lin, R. Jin, A. Wang, S. Zhu and H. Li, *Ceram. Int.*, 2019, **45**, 17996.
49 D. Singh, S. K. Gupta, T. Hussain, Y. Sonvane, P. Gajjar and R. Ahuja, *Energy Fuels*, 2021, **35**, 9001.

50 S. Zhang, M. Xie, F. Li, Z. Yan, Y. Li, E. Kan, W. Liu, Z. Chen and H. Zeng, *Angew. Chem.*, 2016, **128**, 1698.
51 X. Wang, J. Song and J. Qu, *Angew. Chem., Int. Ed.*, 2019, **58**, 1574.
52 D. R. Kripalani, A. A. Kistanov, Y. Cai, M. Xue and K. Zhou, *Phys. Rev. B*, 2018, **98**, 085410.
53 J. Su, T. Duan, W. Li, B. Xiao, G. Zhou, Y. Pei and X. Wang, *Appl. Surf. Sci.*, 2018, **462**, 270.
54 S. Upadhyay and P. Srivastava, *Mater. Chem. Phys.*, 2020, **241**, 122381.
55 L. Zhang, P. Liang, H. B. Shu, X. L. Man, X. Q. Du, D. L. Chao, Z. G. Liu, Y. P. Sun, H. Z. Wan and H. Wang, *J. Colloid Interface Sci.*, 2018, **529**, 426.
56 L. Zhang, W. Zhao, S. Yuan, F. Jiang, X. Chen, Y. Yang, P. Ge, W. Sun and X. Ji, *J. Energy Chem.*, 2021, **60**, 531.
57 L. Ding, Q. Lu, A. D. C. Permana, S. Oswald, M. Hantusch, K. Nielsch and D. Mikhailova, *Energy Technol.*, 2021, **9**, 2001057.
58 F. Hu, H. Peng, T. Zhang, W. Shao, S. Liu, J. Wang, C. Wang and X. Jian, *J. Energy Chem.*, 2021, **58**, 115.
59 J. Zhao, Y. Yang, R. S. Katiyar and Z. Chen, *J. Mater. Chem. A*, 2016, **4**, 6124.
60 X. Gonze, B. Amadon, P.-M. Anglade, J.-M. Beuken, F. Bottin, P. Boulanger, F. Bruneval, D. Caliste, R. Caracas, M. Cote, *et al.*, *Comput. Phys. Commun.*, 2009, **180**, 2582.
61 P. Blochl, *Phys. Rev. B: Condens. Matter Mater. Phys.*, 1994, **50**, 17953.
62 N. A. W. Holzwarth, A. R. Tackett and G. E. Matthews, *Comput. Phys. Commun.*, 2001, **135**, 329.
63 C. Liu and X. Luo, *J. Mater. Chem. B*, 2021, **9**, 2736.
64 J. D. Head and M. C. Zerner, *Chem. Phys. Lett.*, 1985, **122**, 264.
65 W. Lee and X. Yao, *Comput. Mater. Sci.*, 2015, **106**, 76.
66 B. Zhang, H. Zhang, J. Lin and X. Cheng, *Phys. Chem. Chem. Phys.*, 2018, **20**, 30257.
67 A. Zhang and X. Luo, *Mater. Adv.*, 2022, **3**, 5845.
68 M. R. Kaiser, S. Chou, H.-K. Liu, S.-X. Dou, C. Wang and J. Wang, *Adv. Mater.*, 2017, **29**, 1700449.
69 B. Wang, S. M. Alhassan and S. T. Pantelides, *Phys. Rev. Appl.*, 2014, **2**, 034004.
70 C. Barchasz, F. Molton, C. Duboc, J.-C. Leprêtre, S. Patoux and F. Alloin, *Anal. Chem.*, 2012, **84**, 3973.
71 Q. Zhang, X. Zhang, Y. Xiao, C. Li, H. H. Tan, J. Liu and Y. Wu, *ACS Omega*, 2020, **5**, 29272.
72 T.-T. Yu, P.-F. Gao, Y. Zhang and S.-L. Zhang, *Appl. Surf. Sci.*, 2019, **486**, 281.
73 T. Li, C. He and W. Zhang, *J. Mater. Chem. A*, 2019, **7**, 4134.
74 L.-C. Yin, J. Liang, G.-M. Zhou, F. Li, R. Saito and H.-M. Cheng, *Nano Energy*, 2016, **25**, 203.
75 X. Liu, N. Xu, T. Qian, J. Liu, X. Shen and C. Yan, *Nano Energy*, 2017, **41**, 758.
76 V. Kolosnitsyn and E. Karaseva, *Russ. J. Electrochem.*, 2008, **44**, 506.
77 W. Wang, Y. Wang, Y. Huang, C. Huang, Z. Yu, H. Zhang, A. Wang and K. Yuan, *J. Appl. Electrochem.*, 2010, **40**, 321.
78 D. Aurbach, *J. Power Sources*, 2000, **89**, 206.
79 R. Rauh, K. Abraham, G. Pearson, J. Surprenant and S. Brummer, *J. Electrochem. Soc.*, 1979, **126**, 523.
80 L. Lodovico, PhD thesis, dissertation, Karlsruher Institut für Technologie (KIT), Karlsruhe, 2019.
81 U. Blukis, P. H. Kasai and R. J. Myers, *J. Chem. Phys.*, 1963, **38**, 2753.
82 Q. Zhang, Y. Wang, Z. W. Seh, Z. Fu, R. Zhang and Y. Cui, *Nano Lett.*, 2015, **15**, 3780.
83 R. A. Jarrin, *et al.*, PhD thesis, Johns Hopkins University, 2023.
84 T.-Z. Hou, X. Chen, H.-J. Peng, J.-Q. Huang, B.-Q. Li, Q. Zhang and B. Li, *Small*, 2016, **12**, 3283.
85 C. Tang, H.-F. Wang, X. Chen, B.-Q. Li, T.-Z. Hou, B. Zhang, Q. Zhang, M.-M. Titirici and F. Wei, *Adv. Mater.*, 2016, **28**, 6845.
86 K. C. Wasalathilake, M. Roknuzzaman, K. K. Ostrikov, G. A. Ayoko and C. Yan, *RSC Adv.*, 2018, **8**, 2271.